

# Nontrivial in-plane-magnetic-field dependence of THz wave emission from intrinsic Josephson junctions controlled by surface impedance

Yoshihiko Nonomura\*

Computational Materials Science Unit, National Institute for Materials Science, Tsukuba, Ibaraki 305-0047, Japan  
(Dated: December 10, 2018)

In THz wave emission from intrinsic Josephson junctions in in-plane magnetic fields, emission intensity strongly depends on the surface impedance  $Z$  similarly to the case without external magnetic fields. Cavity resonance modes are stabilized for  $Z \geq 3$ , and the fundamental mode gives the strongest emission. As the in-plane magnetic field increases for a fixed number of junctions, dynamical phase transitions seem to occur between the  $\pi$ -phase-kink state, various incommensurate phase-kink states, and in-phase state. As  $Z$  varies, a crossover of the field profile of maximum intensity takes place for  $Z \approx 50$  between characteristic peaks for smaller  $Z$  (typically  $Z \approx 30$ ) and monotonic decrease for larger  $Z$  (typically  $Z \approx 70$ ). The double-peak structure reported in experiments can be explained for  $Z = 30$  by finite-size analysis with respect to number of junctions.

PACS numbers: 74.50.+r, 85.25.Cp, 74.25.Nf

*Introduction.* Although THz wave emission from intrinsic Josephson junctions (IJJs) had been investigated in in-plane magnetic fields, experimental realization of such emission<sup>1</sup> had been quite difficult. Evident emission was observed without external magnetic fields,<sup>2,3</sup> where IJJs have about a thousand of junctions so that the velocity of Josephson plasma mode is already as fast as that of light in IJJs.<sup>4</sup> Then, possible emission states were investigated theoretically, and the uniform in-phase state<sup>5,6</sup> and the  $\pi$ -phase-kink states with symmetry breaking along the  $c$  axis<sup>7,8</sup> have been proposed. The present author showed<sup>9</sup> that these states are both stationary according to the bias current  $J$  and surface impedance  $Z$ . Recently emission in in-plane fields has been investigated again. In an experiment intensity decreases monotonically as the in-plane field increases,<sup>10</sup> while in another experiment the emission intensity seems to have some characteristic peaks in the field profile.<sup>11</sup> The present study suggests that these two experiments may not be contradictory.

*Model and formulation.* As long as thermal fluctuations are not taken into account in the modeling, dimensional reduction along the in-plane magnetic field is justified. When the direction of the magnetic field is chosen as the  $y$  axis, the basic equations are given by<sup>12</sup>

$$\partial_{x'}^2 \psi_l = (1 - \zeta \Delta^{(2)}) (\partial_{t'} E_l' + \beta E_l' + \sin \psi_l - J'), \quad (1)$$

$$\partial_{t'} \psi_l = (1 - \alpha \Delta^{(2)}) E_l', \quad (2)$$

where  $\Delta^{(2)}$  is defined in  $\Delta^{(2)} X_l \equiv X_{l+1} - 2X_l + X_{l-1}$ , and explicit expressions of scaled quantities in the insulating layers are given in Eqs. (7)–(10) of Ref. 9; e.g. length is scaled by the penetration depth  $\lambda_c$  in  $x'$ , time by inverse of the plasma frequency  $\omega_p$  in  $t'$ , and bias current by the critical current  $J_c$  in  $J'$ . In addition to the scaled electric field  $E_l'$ , the scaled magnetic field  $B_l'$  is obtained from  $\partial_{x'} \psi_l = (1 - \zeta \Delta^{(2)}) B_l'$ . Using the material parameters of  $\text{Bi}_2\text{Sr}_2\text{CaCu}_2\text{O}_8$  in Ref. 12, we have a large inductive coupling  $\zeta = 4.4 \times 10^5$  and a small capacitive coupling  $\alpha = 0.1$ , and a scaled conductivity  $\beta = 0.02$  is taken.

Although a thousand of junctions are essential for obtaining the plasma velocity as fast as that of light in IJJs, it is almost impossible to arrive at stationary states for such a large number of junctions numerically at present. Then, the periodic boundary condition along the  $c$  axis is introduced instead, and  $N (\geq 4, N = \text{even})$  junctions are stacked in order to take non-uniformity into account. In such a condition plasma velocity of the stationary state automatically coincides with that of light in IJJs ( $N$  is effectively infinite), though vanishing amplitude of electromagnetic wave (EMW) on surfaces is totally neglected and emitted EMW is parallel to layers. Even if a thousand of junctions are stacked, thickness of IJJ,  $L_z$ , is much smaller than the wavelength of emitted EMW,  $\lambda$ . In such a case emission originates from a point-like source (after two-dimensional reduction, by a line-like source in original three dimensions) and weaker than that parallel to layers. Such effect is approximately included as

$$\partial_{x'} \psi_l = B_{\text{ext}}' + \tilde{B}_l', \quad \partial_{t'} \psi_l = \langle E_l' \rangle + \tilde{E}_l', \quad (3)$$

$$\tilde{E}_l' = \mp Z \tilde{B}_l', \quad Z = z \sqrt{\epsilon_c' / \epsilon_d'}, \quad (4)$$

with the dielectric constants of IJJs  $\epsilon_c'$  and of dielectrics  $\epsilon_d'$ , respectively. Here dynamical parts of scaled boundary magnetic field  $\tilde{B}_l'$  and electric field  $\tilde{E}_l'$  are related with each other by  $z \approx \lambda / L_z$ ,<sup>13</sup> though this naive evaluation of  $z$  might be modified by excess magnetic fields from vertical directions omitted in two-dimensional modeling.<sup>14</sup>

Width of the junction  $L_x = 86 \mu\text{m}$ , which is comparable to experimental scale and  $B_y = 0.02\text{T}$  corresponds to “one Josephson vortex (JV) per layer” for this width, is divided into 80 grids with the RADAU5 ODE solver.<sup>15</sup>

*Numerical results for  $N = 4$ .* First, results for the minimum number of junctions are shown for various values of the surface impedance  $Z$ . In conventional picture of EMW emission from IJJs in in-plane magnetic fields, emission is driven by moving JVs, and the maximum emission is obtained when the distance between JVs coincides with the wavelength of EMW in a junction, which holds for  $Z = 1$ .<sup>16</sup> However, this picture is

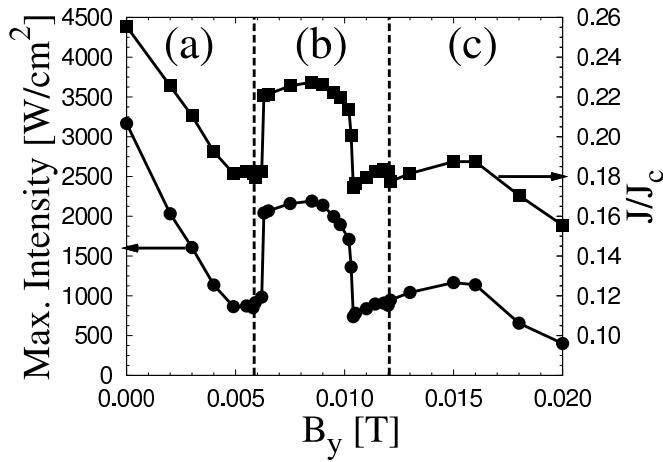


FIG. 1: Field dependence of maximum intensity in the  $n = 1$  cavity resonance mode for  $N = 4$  (circles) at the optimal bias current (squares). Dips of the curves stand for the dynamical phase transitions between the (a)  $\pi$ -phase-kink ( $\pi$ -PK), (b) incommensurate-phase-kink (IPK), and (c) in-phase states.

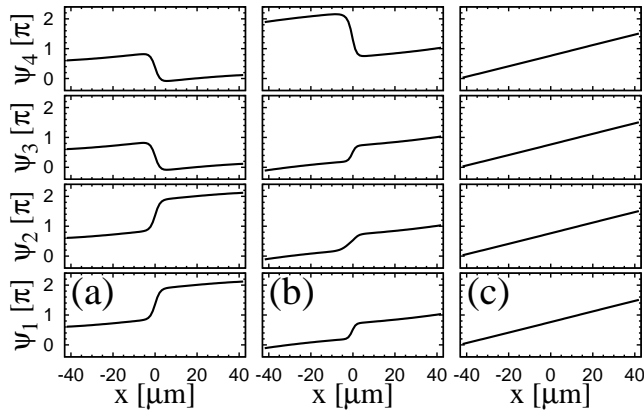


FIG. 2: Snapshots of gauge-invariant phase differences in all junctions for  $N = 4$  at (a)  $B_y = 0.003\text{T}$ ,  $J = 0.210J_c$  (in the  $\pi$ -PK state; two  $\pm\pi$  kinks), (b)  $B_y = 0.009\text{T}$ ,  $J = 0.226J_c$  (in the IPK state; three  $+(1/2)\pi$  kinks and one  $-(3/2)\pi$  kink), and (c)  $B_y = 0.015\text{T}$ ,  $J = 0.187J_c$  (in the in-phase state).

the case only for in-plane magnetic fields applied to the in-phase state, which is stable only for small  $Z$  without external magnetic fields.<sup>9</sup> For  $Z \geq 3$ , emission from the cavity-resonance mode becomes stronger than that from the driven-JVs mode, and the fundamental mode becomes stronger than higher-harmonic modes. Then, only the fundamental mode is considered hereafter.

(I) *detailed results for  $Z = 30$ .* As a typical value of the surface impedance,  $Z = 30$  is chosen. Maximum emission intensity and corresponding bias current are plotted versus in-plane magnetic field in Fig. 1. Procedure to obtain this figure is as follows: (1) to fix the in-plane magnetic field, (2) to sweep the bias current and evaluate stationary emission intensity, and (3) to draw the optimal set of stationary values. Two dips in this figure divide the

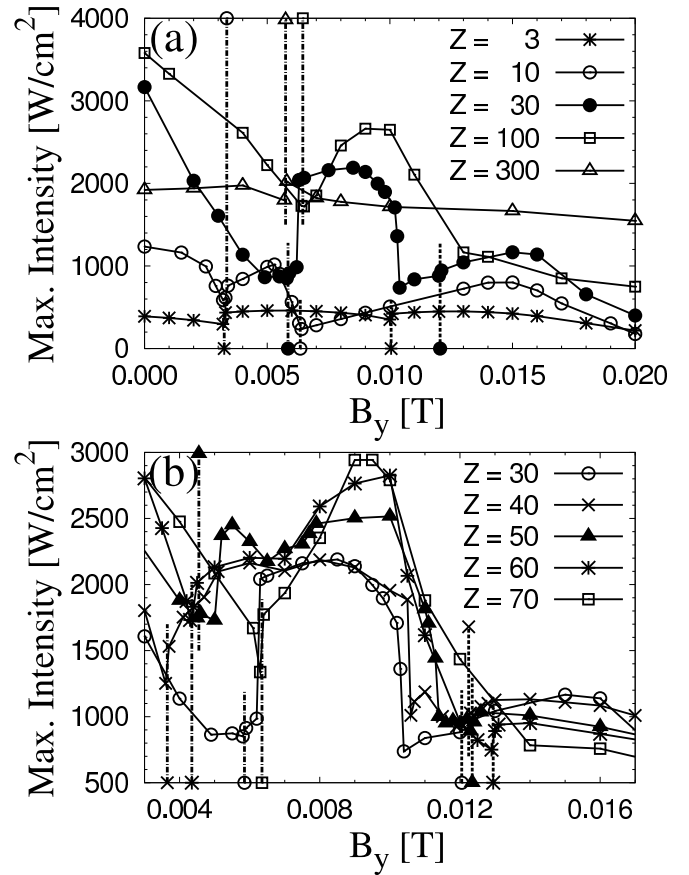


FIG. 3: Field dependence of maximum intensity for  $N = 4$  for various values of the surface impedance  $Z$ : (a) for  $Z = 3$  (stars), 10 (open circles), 30 (full circles), 100 (open squares) and 300 (open triangles); (b) expanded figure for  $Z = 30$  (open circles), 40 (saltires), 50 (full triangles), 60 (stars) and 70 (open squares). In each figure dash-dotted and dashed lines denote boundaries between the  $\pi$ -PK and IPK states and between the IPK and in-phase states, respectively.

three dynamical states characterized by the structure of gauge-invariant phase difference as displayed in Fig. 2: (a) the  $\pi$ -phase-kink ( $\pi$ -PK) state stable without external magnetic fields, (b) the incommensurate-phase-kink (IPK) state in the intermediate field region, and (c) the in-phase state. Field dependence of the current deriving the maximum intensity (optimal current) is also plotted in Fig. 1 by squares. Its shape is quite similar to that of the maximum intensity, and this field profile will not be shown hereafter. The maximum intensity jumps up and down almost discontinuously inside (not on the boundaries) of the IPK state, which will be discussed later.

(II) *results for other  $Z$ .* Field dependence of maximum intensity for  $N = 4$  is given in Fig. 3(a) for  $Z = 3, 10, 30, 100$  and  $300$  together with transition fields for each  $Z$  (dash-dotted lines between the  $\pi$ -PK and IPK states, and dashed lines between the IPK and in-phase states). This figure clearly indicates strong  $Z$  dependence of the field profile of maximum intensity. For  $Z = 10$  and  $30$ ,

the first emission peak appears between the two ( $\pi$ -PK-IPK and IPK-in-phase) transition fields, and there exists the second peak at  $B_y \approx 0.015\text{T}$  in the in-phase state. For  $Z = 100$  and  $300$ , on the other hand, the IPK-in-phase transition field does not locate for  $B_y \leq 0.02\text{T}$ , and no emission peak exists at  $B_y \approx 0.015\text{T}$ . These facts suggest that there would be a crossover of the field profile of maximum intensity between  $Z = 30$  and  $100$ .

Then,  $Z$  dependence of the field profile of maximum intensity is displayed for  $Z = 30, 40, 50, 60$  and  $70$  in Fig. 3(b) together with the transition fields for each  $Z$ . Although values of the  $\pi$ -PK-IPK transition field are close for  $Z = 30$  and  $70$ , this transition field is independent of the emission peak for  $Z = 30$ , while it is linked with the peak for  $Z = 70$ . This behavior changes between  $Z = 50$  and  $60$ . There exists similar change in behavior of the IPK-in-phase transition field between  $Z = 50$  and  $60$ . In addition, the characteristic peak at  $B_y \approx 0.015\text{T}$  is visible up to  $Z = 40$ , and it almost disappears for  $Z \geq 50$ . To summarize, there seems to exist a crossover in the field profile of maximum intensity at  $Z \approx 50$ .

*Numerical results for various number of junctions.* In order to compare the above results with experiments, we should clarify dependence of numerical results on the number of junctions  $N$ , and distinguish general properties independent of  $N$  from special properties only for small  $N$ . As a typical value of the surface impedance  $Z = 30$  is chosen again, and field dependence of maximum intensity for  $N = 4$  (full circles),  $6$  (open circles),  $8$  (open squares) and  $12$  (open triangles) is displayed in Fig. 4(a) together with the onset fields of the  $\pi$ -PK state (dash-dotted lines) and the  $\pi/2$ -PK state (dashed lines) and the first emission peaks (arrows). In order to show examples of various IPK states for larger  $N$  explicitly, the data for  $N = 12$  are extracted in Fig. 4(b), where the regions “ $\pi$ ”, “ $\frac{5}{6}\pi$ ”, “ $\frac{2}{3}\pi$ ”, “ $\frac{\pi}{2}$ ”, “ $\frac{\pi}{3}$ ”, “ $\frac{\pi}{6}$ ” and “0” represent the  $[\pi\text{-kink} \times 6 - \pi\text{-kink} \times 6]$ ,  $[\frac{5}{6}\pi\text{-kink} \times 7 - \frac{7}{6}\pi\text{-kink} \times 5]$ ,  $[\frac{2}{3}\pi\text{-kink} \times 8 - \frac{4}{3}\pi\text{-kink} \times 4]$ ,  $[\frac{\pi}{2}\text{-kink} \times 9 - \frac{3}{2}\pi\text{-kink} \times 3]$ ,  $[\frac{\pi}{3}\text{-kink} \times 10 - \frac{5}{3}\pi\text{-kink} \times 2]$ ,  $[\frac{\pi}{6}\text{-kink} \times 11 - \frac{11}{6}\pi\text{-kink} \times 1]$  and in-phase states, respectively. All possible combinations of IPK states appear as the in-plane magnetic field increases, and small jump or dip of the maximum intensity is observed at each transition field.

Finally, the onset fields of the  $\pi$ -PK and  $\pi/2$ -PK states and the field at the first emission peak are plotted versus  $1/N$  in Fig. 5. These data strongly suggest that the onset field of the  $\pi$ -PK state seems to converge to  $B_y = 0$  in the  $N \rightarrow \infty$  limit (dash-dotted line). When these four data points are fitted by  $B_y(N) = a/N + b$ , we have  $b = 0.0002 \pm 0.0002$  [T]. On the other hand, the onset field of the  $\pi/2$ -PK states converges to a nonvanishing value (dashed line) with the same assumption. Similar preliminary results can be obtained for other IPK states, though the number of data is still limited. Moreover, the in-plane fields at the first emission peak coincide with each other for  $N = 8$  and  $12$ , and the extrapolated value is expected to be nonvanishing for large  $N$ .

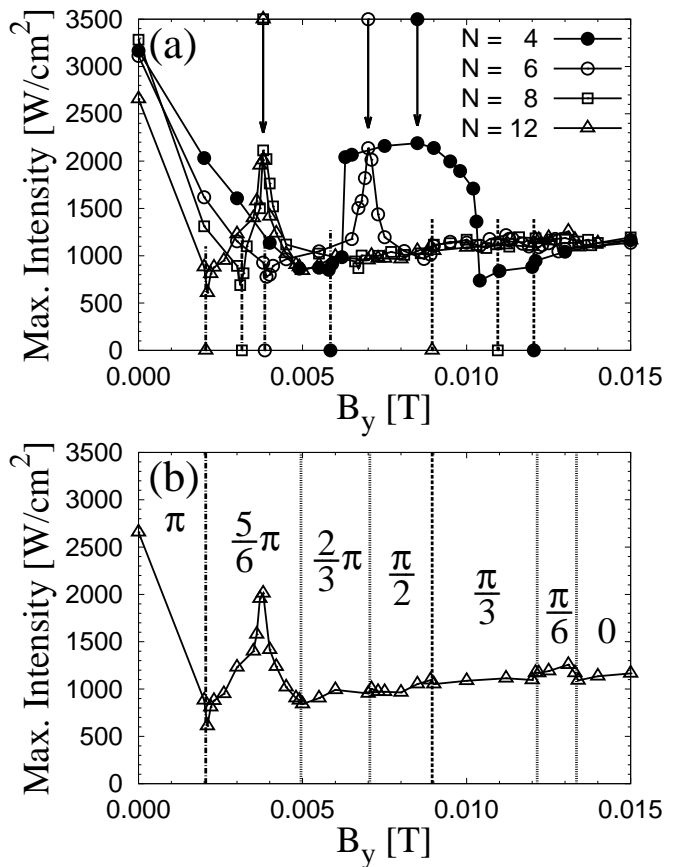


FIG. 4: (a) Field dependence of maximum intensity for  $Z = 30$  for various number of junctions  $N$ : for  $N = 4$  (full circles),  $6$  (open circles),  $8$  (open squares) and  $12$  (open triangles). Dash-dotted and dashed lines denote boundaries between the  $\pi$ -PK and the next IPK states and between the  $\pi/2$ -PK and the next IPK states, respectively. Arrows stand for the first peaks of the maximum intensity. (b) Field dependence of the data for  $Z = 30$  and  $N = 12$  is extracted in order to display various IPK states explicitly (“0” means the in-phase state).

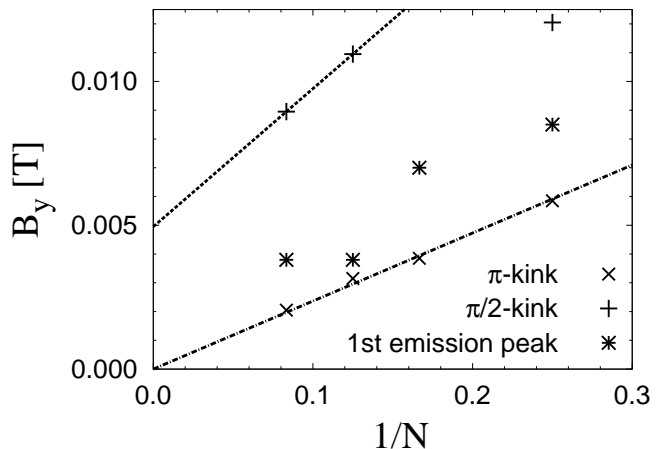


FIG. 5: Junction-number dependence of onset fields of the  $\pi$ -PK state (crosses) and the  $\pi/2$ -PK state (pluses), and of fields at the first emission peak (stars) for  $Z = 30$ . Dash-dotted and dashed lines are drawn as guide for eyes.

*Discussions.* Even if the periodic boundary condition is applied along the  $c$  axis, dependence on the number of junctions  $N$  is still not negligible as shown above. Since number of junctions in experiments is of order of  $N \approx 1000$ , extrapolation to large  $N$  is crucial for reproducing experiments. On the other hand, maximum number of treatable  $N$  is still not so large. CPU time is proportional to  $N^3$  in this calculation, and relaxation time to reach stationary states rapidly increases as  $N$  or  $Z$  increases. For example,  $t = 5 \times 10^3 \omega_p^{-1}$  is long enough for  $Z = 10$  and  $N = 12$ , but  $t = 2 \times 10^4 \omega_p^{-1}$  is at least necessary for  $Z = 30$  and  $N = 12$ . Therefore, calculation for  $N \geq 16$  or  $Z = 70$  in the same scale is difficult at present.

Then, alternative approach to numerical data is required, and the data for  $N = 4$  around the crossover region given in Fig. 3(b) are reconsidered. The onsets of the first emission peak for  $Z \leq 50$  do not coincide with the boundaries of the IPK state including this peak, which suggests that the first emission peak is not related with the dynamical phase transitions in this parameter region. On the other hand, the onsets and the dynamical phase transitions seem to synchronize for  $Z \geq 60$ . After extrapolating to the large- $N$  limit, the zero-field peak and the dip at the onset of the  $\pi$ -PK state might cancel with each other and the  $N$ -independent first emission peak at  $B_y \approx 0.003\text{T}$  and the broad second emission peak at  $B_y \approx 0.015\text{T}$  in the in-phase state might remain for  $Z \leq 40$ , while for  $Z \geq 60$  both the onset of the  $\pi$ -PK state and the first emission peak shrink to zero field, and merely monotonically-decreasing field dependence of the higher-field side of the first emission peak remains.

The picture that a crossover between two different types of emission takes place at  $B_y \approx 50$  can also be justified by the shape of emission peaks for  $N = 4$  by itself. The peak has sharp edges for  $Z = 30$ , broadens to lower fields for  $Z = 40$ , and splits for  $Z = 50$ . The higher-field peak grows while lower-field one shrinks for  $Z = 60$ , and the lower-field peak vanishes for  $Z = 70$ .

These descriptions for large- $N$  behaviors of the present modeling seem consistent with the preceding experiments, namely the one by Yamaki *et al.*<sup>11</sup> with the case for  $Z \leq 40$ , and the one by Welp *et al.*<sup>10</sup> with the case for  $Z \geq 60$ . If they are the case, the discrepancy between these two experiments is not serious contradiction but consequence of a little difference of experimental con-

ditions to vary the surface impedance in the vicinity of the crossover point  $Z \approx 50$ . This argument also suggests that values of  $Z$  in experiments may be much smaller than that naively expected from the relation  $z \approx \lambda/L_z$  or  $Z \approx 500$ . It means that the argument by Tachiki *et al.*<sup>14</sup> that  $Z$  is effectively reduced by magnetic fields from vertical directions may be partially true, but that such effect is not so strong as they considered; they argued that  $Z$  may be reduced so much that the in-phase emission is observed. Further studies to handle much larger numbers of junctions numerically or to manipulate the surface impedance experimentally are still necessary.

Finally, physical meaning of the IPK states is considered. When the in-plane magnetic field is applied, IPK between  $0$  and  $+\pi$  coupled with the in-plane field could be identified with “ $+\pi$ -PK”, and IPK between  $-2\pi$  and  $-\pi$  coupled with the in-plane field with “ $-\pi$ -PK”. From this point of view, unbalance of “ $+\pi$ -PKs” and “ $-\pi$ -PKs” represents nonvanishing in-plane fields, and the in-phase state would be stable for  $B_y \geq 0.01\text{T}$  ( $0.5\text{JV}$  per layer). The extrapolated onset field  $B_y \approx 0.005\text{T}$  of the  $\pi/2$ -PK state (Fig. 5) is consistent with this picture.

*Summary.* THz wave emission from intrinsic Josephson junctions in in-plane magnetic fields is investigated numerically. Cavity-resonant emission is observed for  $Z \geq 3$  similarly to the case without external fields, and the  $n = 1$  emission mode is the strongest. There occur field-induced dynamical phase transitions between the  $\pi$ -phase-kink ( $\pi$ -PK) state, various incommensurate-phase-kink (IPK) states and in-phase state as the in-plane magnetic field increases. Investigation on dependence of physical quantities on junction numbers  $N$  suggests that the  $\pi$ -PK state may be stable only without external magnetic fields for large  $N$ . In the field profile of maximum intensity there exist a crossover between two characteristic peaks at  $\sim 0.15$  and  $\sim 0.75\text{JV}$  per layer<sup>11</sup> for  $Z \leq 40$  and monotonic decrease<sup>10</sup> for  $Z \geq 60$ , which suggests that controversy of the field profile in recent experiments<sup>10,11</sup> may be explained by slight difference in the surface impedance due to experimental conditions.

*Acknowledgments.* The present work was partially supported by Grant-in-Aids for Scientific Research (C) No. 20510121 from JSPS.

\* Electronic address: nonomura.yoshihiko@nims.go.jp

<sup>1</sup> M.-H. Bae *et al.*, Phys. Rev. Lett. **98**, 027002 (2007).

<sup>2</sup> L. Ozyuzer *et al.*, Science **318**, 1291 (2007); see also K. Lee *et al.*, Phys. Rev. B **61**, 3616 (2000).

<sup>3</sup> K. Kadowaki *et al.*, Physica C **468**, 634 (2008).

<sup>4</sup> S. Sakai *et al.*, J. Appl. Phys. **73**, 2411 (1993); S. Sakai *et al.*, Phys. Rev. B **50**, 12905 (1994).

<sup>5</sup> H. Matsumoto *et al.*, Physica C **468**, 654, 1899 (2008).

<sup>6</sup> T. Koyama *et al.*, Phys. Rev. B **79**, 104522 (2009).

<sup>7</sup> S. Lin and X. Hu, Phys. Rev. Lett. **100**, 247006 (2008).

<sup>8</sup> A. E. Koshelev, Phys. Rev. B **78**, 174509 (2008).

<sup>9</sup> Y. Nonomura, Phys. Rev. B **80**, 140506(R) (2009).

<sup>10</sup> U. Welp *et al.*, on the APS March Meeting 2009, D34-1.

<sup>11</sup> K. Yamaki *et al.*, Physica C **470**, S804 (2010).

<sup>12</sup> M. Tachiki *et al.*, Phys. Rev. B **71**, 134515 (2005).

<sup>13</sup> A. E. Koshelev and L. N. Bulaevskii, Phys. Rev. B **77**, 014530 (2008).

<sup>14</sup> M. Tachiki *et al.*, Phys. Rev. Lett. **102**, 127002 (2009).

<sup>15</sup> <http://www.unige.ch/~hairer/software.html>

<sup>16</sup> Y. Nonomura, J. Phys.: Conf. Ser. **150**, 052191 (2009).